Journal of Power Sources 233 (2013) 320–325

Contents lists available at SciVerse ScienceDirect

Journal of Power Sources

journal homepage: www.elsevier.com/locate/jpowsour

Dye-sensitized solar cells with high-performance polyaniline/multi-wall carbon nanotube counter electrodes electropolymerized by a pulse potentiostatic technique

Yaoming Xiao [a,b], Jeng-Yu Lin [b,*,1], Jihuai Wu [a], Sheng-Yen Tai [b], Gentian Yue [a,b], Tsung-Wu Lin [c]

[a] Institute of Materials Physical Chemistry, Huaqiao University, Quanzhou, Fujian 362021, China
[b] Department of Chemical Engineering, Tatung University, No. 40, Sec. 3, ChungShan North Rd., Taipei City 104, Taiwan
[c] Department of Chemistry, Tunghai University, No. 181, Sec. 3, Taichung Port Rd., Taichung City 40704, Taiwan

HIGHLIGHTS

- High-performance PANI/MWCNT composite CE was incorporated for Pt-free DSCs.
- The thickness of PANI thin film coated around the MWCNTs was 45 nm.
- Enhanced electrocatalytic activity for the PANI/MWCNT CE was demonstrated.
- The efficiency of the Pt-free DSC reached 6.25% based on the PANI/MWCNT CE.

ARTICLE INFO

Article history:
Received 23 September 2012
Received in revised form
4 January 2013
Accepted 20 January 2013
Available online 28 January 2013

Keywords:
Polyaniline
Carbon nanotube
Counter electrode
Dye-sensitized solar cell

ABSTRACT

Strong scientific interests focus on the investigation of Pt-free counter electrodes (CEs) for their application in dye-sensitized solar cells (DSCs). Here we demonstrate the synthesis of a high-performance polyaniline/multi-wall carbon nanotube (PANI/MWCNT) nanocomposite CE via electrophoresis of MWCNTs onto a fluorinated tin oxide (FTO) substrate and then subjected to PANI electropolymerization by using the pulse potentiostatic method. The resultant rough PANI thin film around the MWCNT is ~45 nm in thickness. Cyclic voltammetry, electrochemical impedance spectroscopy, and Tafel polarization measurements reveal that PANI/MWCNT CE possesses an enhanced electrocatalytic activity for I_3^- reduction compared to PANI and MWCNT CEs due to its intrinsic superior electrocatalytic activity of the PANI material and high surface area of the MWCNTs. The DSC assembled with the pulsed PANI/MWCNT CE exhibits the superior photovoltaic conversion efficiency of 6.24% (compared to 5.18% for DSCs with PANI CE or 6.05% for DSCs with Pt CE) under full sunlight illumination (100 mW cm^{-2}, AM1.5 G). Therefore, the high-performance PANI/MWCNT can be considered as a cost-effective CE alternative for DSCs.

1. Introduction

In 1991, the seminal paper by Grätzel and his co-worker [1] on dye-sensitized solar cells (DSCs) opened up the possibility to the use of solar electricity production facilities. The DSCs have attracted a great deal attention due to their low cost and relatively high energy conversion efficiency [2,3]. In a typically DSC, a counter electrode (CE) is employed to speed up the reduction of I_3^- to I^-. To date, platinum (Pt) thin film coated on transparent conductive oxides, such as indium-doped tin oxide (ITO) or fluorine-doped tin oxide (FTO), has been generally adopted as the CEs in DSCs due to their high conductivity, electrocatalytic activity and chemical stability [4,5]. Nevertheless, Pt is an expensive noble metal in DSCs [6]. Evolution of the CEs with other cost-effective alternatives is required to reduce production cost of DSCs. Some other materials such as carbon materials [7,8], conducting polymers [9–12], and composites of the previous materials [13–16] have been employed for the CEs to replace the Pt.

Among them, multi-wall carbon nanotubes (MWCNTs) have attracted lots of attention due to their characteristics of highly specific surface, rapid electron transfer nature and excellent

* Corresponding author.
E-mail addresses: jylin@ttu.edu.tw, d923615@gmail.com (J.-Y. Lin).
[1] Tel.: +866 22592 5252x2561 119; fax: +866 22586 1939.

0378-7753/$ – see front matter © 2013 Elsevier B.V. All rights reserved.
http://dx.doi.org/10.1016/j.jpowsour.2013.01.116

mechanical strength [17]. Nevertheless, their electrocatalytic activities for I_3^- reduction are not satisfactory [18,19]. Additionally, Li et al. [11] reported that environmentally stable and low cost polyaniline (PANI) was synthesized as the CE for DSCs through a chemical polymerization and achieved an excellent electrocatalytic activity and stability. Compared with the chemical polymerization method, the electropolymerization methods belong to considerably simpler and more cost-effective technique to obtain conducting polymers with the controllable surface morphology and well adhesion on the substrate surface. Chen et al. [15] revealed that PANI/carbon prepared using a potentiodynamic method, was serviced in the DSC as a CE and achieved an improved cell performance. Huang et al. [14] employed a reflux method to form the nanographite/aniline (NG/ANI) monomer for the constant potential electropolymerization of the NG/PANI composite films. These studies revealed that the superior electrocatalytic activity and conductivity of the PANI/carbon materials CEs render high photovoltaic performance to the DSCs. Furthermore, the pulse electropolymerization of conducting polymers has numerous advantages in terms of controlled particle size and uniformity by means of overcoming diffusion-limited mass transport of monomers to the electrode surface from the bulk solution [16,20,21].

In this study, we first used the pulse electropolymerization to synthesize a PANI film on the MWCNT/FTO substrate and employed it as a CE for Pt-free DSCs. The DSC assembled with the PANI/MWCNT CE exhibited an enhanced photovoltaic conversion of 6.24% to those of the DSCs with the Pt, MWCNT, and PANI CEs.

2. Experimental

2.1. Fabrication of CEs

Raw MWCNTs (Purity: >99.5%; Average diameter: 40–90 nm; Length: >10 um; Golden Innovation Business Co.) were refluxed in a 3:1 mixture of H_2SO_4 (98%) and HNO_3 (78%) at 120 °C for 2 h to oxidize the graphitic sp^2 carbon into a −COOH functional group on the side walls of the MWCNTs. The oxidized MWCNTs were further filtered by suction filtration, washed thoroughly with deionized water, and suspended in a 1:1 mixture of acetone and ethanol by ultrasonication for 2 h. The aqueous MWCNT suspensions of 0.5 mg mL^{-1} concentrations were used for the electrophoresis experiments. Cleaned fluorinated tin oxide (FTO) glass substrates (NSG, 13 Ω/□) and a Pt sheet (2 cm^2) were used as a working electrode and a counter electrode, respectively. A constant potential of 18 V vs. open-circuit potential was employed for 30 s [18]. Subsequently, the resulting MWCNT CEs (~0.5 μm in thickness) were dried at 50 °C for 10 min.

The pulse potentiostatic electropolymerization of PANI onto FTO glass or MWCNT/FTO glass substrates was carried out using a Zahner electrochemical workstation (Zahner-Elektrik Gmbh & Co. KG, Germany) from an aqueous solution containing 1.0 M ANI monomer (Arcos, 99%) and 2.0 M HCl in a three compartment cell at ambient atmosphere, which was controlled by ZAHNER THALES software. The parameters for PANI CE were selected under 1.1 V pulse-on potential, 0 V pulse-reversal potential, 1 s pulse-on period, 0.5 s pulse-reversal period, and total 150 s duration time. Cleaned FTO glass substrates and a Pt wire were used as a working electrode and a counter electrode, respectively, in addition to a saturated silver/silver chloride (Ag/AgCl) reference electrode. The PANI/MWCNT CEs were fabricated at the same experiment parameters as the PANI preparation, but changing the FTO glass substrates to MWCNT/FTO glass substrates. The obtained PANI and PANI/MWCNT CEs were rinsed in distilled water and dried under a cool air flow. For comparison, a Pt CE was prepared by thermal decomposition of H_2PtCl_6 on FTO glass at 390 °C.

2.2. Characterization

The surface morphologies of the PANI and PANI/MWCNT CEs were observed using a field-emission scanning electron microscopy (FESEM; JSM-7600F). Fourier transform infrared spectra (FTIR) of samples were recorded on a Perkin Elmer Spectrum Gx FTIR Spectrometer using KBr as pellets. The cyclic voltammetry (CV) for I^-/I_3^- system was conducted using a computer-controlled potentiostat (PGSTAT320N, Autolab) in the potential interval ranging from −0.4 V to 0.4 V vs. Pt at a scan rate of 10 mV s^{-1}. CV tests were conducted, in which an as-prepared CE was taken as the working electrode in a three-electrode one-compartment cell, a 4 cm^2 Pt sheet auxiliary electrode and a Pt wire reference electrode in a 3-methoxypropionitrile solution consisting of 50 mM LiI, 10 mM I_2, and 500 mM $LiClO_4$. The electrochemical impedance spectroscopy (EIS) and Tafel measurements were carried out with two identical electrodes, which were sealed with a thermoplastic hot-melt Surlyn leaving an exposed area of 0.64 cm^2. The detailed procedure for the fabrication of the symmetric dummy cell has been reported elsewhere [22,23]. The EIS analysis was carried out. The impedance studies were carried out using the Zahner electrochemical workstation at open-circuit condition, and the impedance data covered a frequency range of 10^{-1}–10^6 Hz with zero bias potential and 10 mV of amplitude, under a dark condition. The resultant impedance spectra were analyzed using the Z-view software. The Tafel polarization curves were measured using an electrochemical workstation system (CHI608, USA) at a scan rate of 10 mV s^{-1}. The liquid redox electrolyte composed of 1 M 1,3-dimethylimidazolium iodine (Merck), 0.15 M iodine (J.T. Baker), 0.5 M 4-tertpbutylpyridine (Aldrich), and 0.1 M guanidine thiocyanate (Aldrich) in 3-methoxypropionitrile (Acros) solution was employed in the EIS, Tafel polarization, and the following photoelectrochemical tests.

2.3. Photoelectrochemical measurements

The TiO_2 photoanode was prepared according to our previous reports [24,25]. The resulting TiO_2 photoanode was further sensitized by immersing it into a 0.3 mM ethanolic solution of N719 dye ([cis-di(thiocyanato)-*N*,*N*′-bis (2,2′-bipyridyl-4-carboxylic acid-4-tetrabutylammonium carboxylate) ruthenium (II)]; Everlight Chemical Industry Co.) for 12 h, followed by air drying. After dye adsorption, the TiO_2 photoanode was assembled with a CE. Then the electrolyte was injected into the cell. The photocurrent density–voltage characteristic was made using a computer-controlled Keithley 2400 source meter under illumination by a solar simulator (Yamashita Denso YSS-150A). The incident light intensity and the active cell area were 100 mW cm^{-2} (AM1.5) and 0.28 cm^2, respectively.

3. Results and discussion

The FE-SEM images of the FTO, MWCNT, PANI, and PANI/MWCNT CEs are shown in Fig. 1. Fig. 1a shows the bare FTO glass. For the MWCNT CE (Fig. 1b), it can be found that the fiber-like MWCNTs film was formed onto the FTO glass substrate after the electrophoresis deposition. Fig. 1c shows the PANI film composed of highly uniform and rough nanofibers (diameter of 90 nm) prepared by using the pulse potentiostatic method. To effectively utilize the high surface area of the MWCNTs and improve the adhesion between the MWCNT and the FTO glass substrate, the pulse electropolymerization of PANI thin film was further carried out on the MWCNTs/FTO surfaces. Furthermore, the original diameter of MWCNTs was about 90 nm. Notably; after electropolymerization of PANI onto the MWCNTs, the diameter of MWCNT increased to

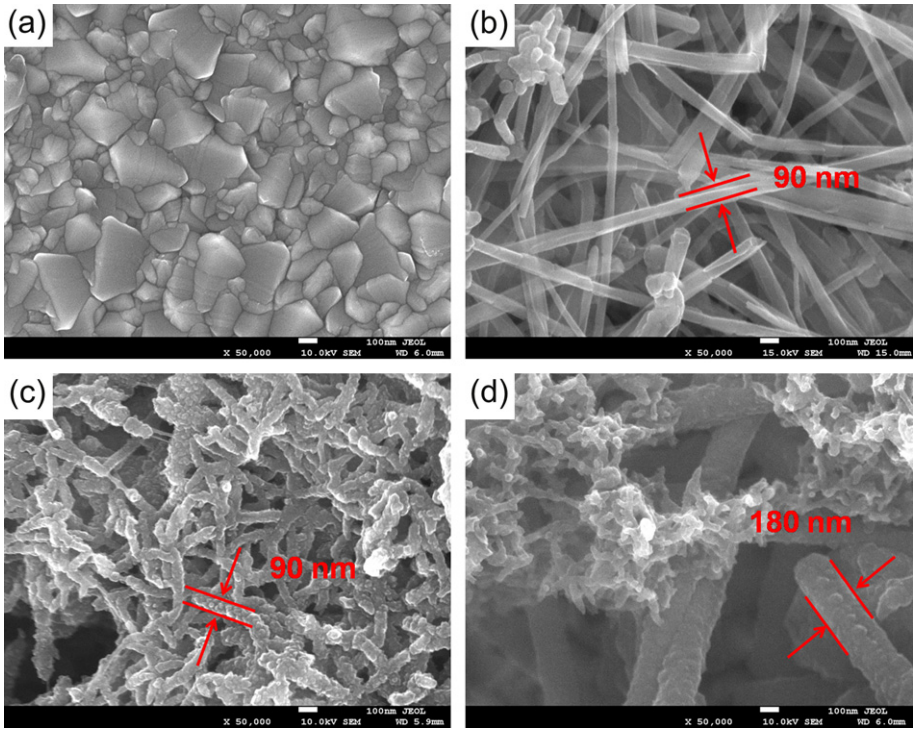

Fig. 1. FE-SEM images of the (a) FTO, (b) MWCNT, (c) PANI, and (d) PANI/MWCNT CEs, respectively.

180 nm, therefore PANI thin film in the thickness of ~45 nm was coated around the MWCNT (Fig. 1d). Furthermore, some PANI nanofibers were observed to be deposited on the MWCNTs, thus possibly improving the adhesion of the MWCNTs on the FTO glass substrates and the electrical transport connection between PANI-coated MWCNTs.

Fig. 2 shows the FTIR spectra of the MWCNT, PANI, and PANI/MWCNT, respectively. As shown in the MWCNT curve, the absorption bands at 1581 and 1223 cm^{-1} are associated with the stretching of the carbon nanotube backbone; two bands appeared at 1717 and 1384 cm^{-1} are attributed to the C═O stretching vibrations and hydroxyl groups (−OH) bending deformation of the carboxylic groups (−COOH) of acid-oxidized MWCNTs, respectively

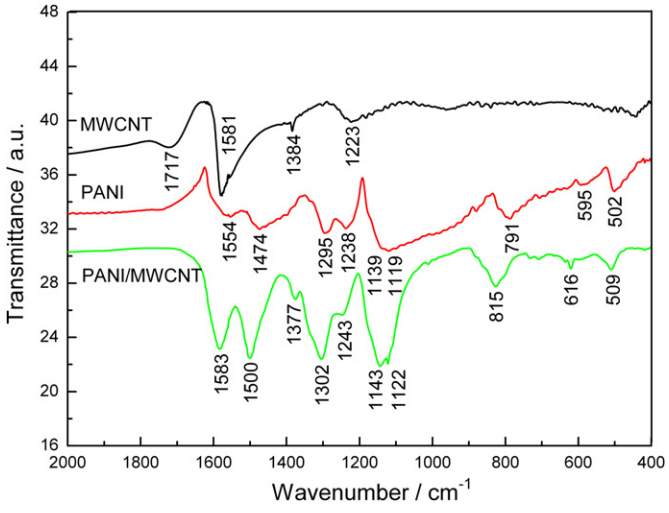

Fig. 2. FTIR spectra of the MWCNT, PANI, and PANI/MWCNT, respectively.

[26,27]. The characteristic absorption bands of the PANI nanofiber appeared at 1554 and 1474 cm^{-1} are indexed to the C═C stretching of quinoid ring and benzenoid deformation of PANI, respectively. We also observed C—N stretching mode and bending mode at 1295 and 1238 cm^{-1}, respectively. The C—H bending of the quinoid ring appears at 1139 and 1119 cm^{-1} [28]. In the PANI/MWCNT curve, the absorption bands at 1717, 1581, 1384 and 1223 cm^{-1} disappeared or receded can be possibly ascribed to the fact that the acid-oxidized MWCNTs were completely wrapped with the PANI thin films. Thus, the FE-SEM and FTIR results indicate that the PANI films were successfully electropolymerized on the surfaces of MWCNTs and FTO glass substrates. Fig. 3 further shows a schematic diagram of the pulse potentiostatic electropolymerization of PANI onto the MWCNTs and FTO glass. It is interesting that the acid-oxidized MWCNT has a −COOH functional group on the side walls of the nanotubes, which can ionize out MWCNT-COO^- negative ion in the aqueous solution. In general, the ANI can be easily protonized to $ANIH^+$ positive ion. Therefore, the resultant $ANIH^+$ positive ion can be easily adsorbed onto the surface of the acid-oxidized MWCNT via the electrostatic interaction; on the other hand, the acid-oxidized MWCNT has large specific surface area to catch hold of lots of $ANIH^+$ positive ions, thus the PANI film can be electropolymerized around the acid-oxidized MWCNT preferentially and thoroughly. With continuing growth, the PANI makes a powerful adhesion among the MWCNTs, FTO glass, and PANI.

Fig. 4 shows the cyclic voltammogram for the Pt, MWCNT, PANI, and PANI/MWCNT CEs, respectively. The CEs show a pair of oxidation and reduction peaks, the redox pair is attributed to the reaction of $I_3^- + 2e^- \rightarrow 3I^-$, which directly affects the DSC performance [29]. The peak-to-peak separation (E_{pp}) and peak current density, which is negatively correlated with the standard electrochemical rate constant of a redox reaction, are two critical parameters for comparing electrocatalytic activities of different CEs [30]. No significant reduction peak was observed for the MWCNT CE in this potential interval, suggesting the reduction reaction of I_3^- to I^- on MWCNT CE

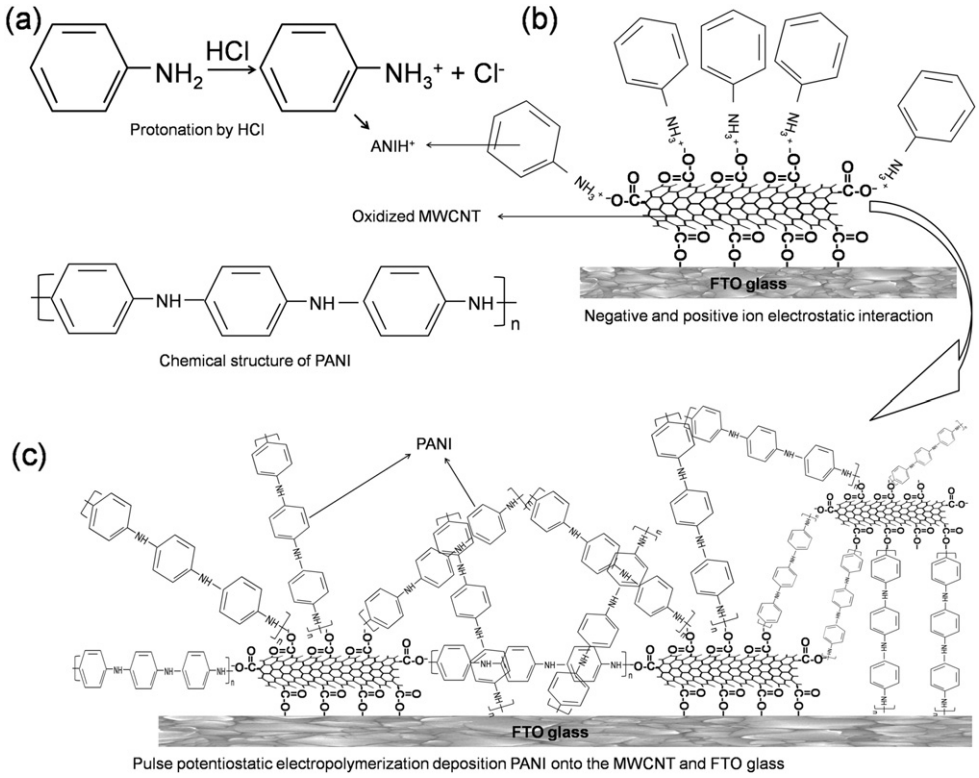

Fig. 3. Schematic diagram of the deposition mechanism for the pulse potentiostatic electropolymerization of PANI onto the MWCNTs and FTO glass.

is remarkably slower. The cathodic peak potentials of the reduction reaction on the PANI and PANI/MWCNT CEs are more negative than that of the Pt CE, one possible explanation may be ascribed to the adsorption of electrolyte, like 4-tert-butylpyridine onto the PANI surface as well as the carbon materials [31]. The E_{pp} value (shown in Table 1) decreases in the order of PANI (398 mV) > PANI/MWCNT (292 mV) > Pt (265 mV), indicating an inverse order of electrocatalytic activity. However, the cathodic current density increases in the order of Pt < PANI < PANI/MWCNT, resulting in a same order of electrocatalytic activity, which could be explained by the reason that the active surface area increases in the same order (discussed at the posterior EIS section). Overall consideration of the E_{pp} and peak current density, the PANI/MWCNT CE has slightly higher E_{pp} value but much larger cathodic current density than that of the Pt CE, demonstrating a higher electrocatalytic activity than that of the Pt CE. The enhanced electrocatalytic activity can be attributed to its highly specific surface and rapid electron transfer nature from the MWCNT, and intrinsically excellent electrocatalytic activity from PANI.

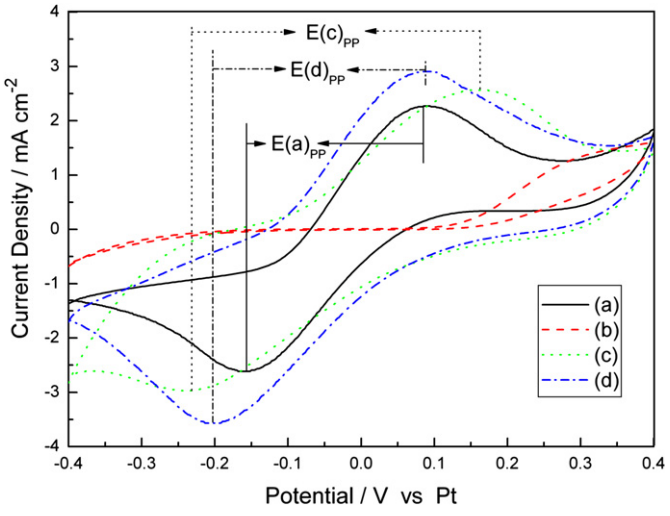

Fig. 4. CVs of the (a) Pt, (b) MWCNT, (c) PANI, and (d) PANI/MWCNT CEs, respectively.

To further elucidate the electrocatalytic activities of different CEs on the I_3^- reduction, EIS measurements were carried out using symmetric cells fabricated with two identical electrodes. The Nyquist plots (Fig. 5) for symmetric cells with different CEs illustrate impedance characteristics. The intercept of the real axis at high frequency is the ohmic series resistance (R_S) including the sheet resistance of two identical CEs and the electrolytic resistance. The semicircle at high frequency refers to the charge-transfer resistance (R_{CT}) of the I_3^- reduction at the electrolyte/CE interface, which changes inversely with the catalytic activity of different CEs on the I_3^- reduction, and the semicircle at low frequency represents the Warburg impedance (W), which corresponds to the diffusion resistance of the I^-/I_3^- redox species. The constant phase element (CPE) is frequently used as a substitute for the capacitor in an equivalent circuit to fit the impedance behavior of the electrical double layer more accurately when the double layer does not behave as an ideal capacitor [32]. It should be noted that the Warburg impedance of the polymer-based CE originating from the charge transport in the catalyst cannot be ignored due to its low electrical conductivity, compared with that of the Pt catalyst. Thus, the element (W_{cat}) representing the Warburg impedance from the charge transport resistance in the PANI film should be incorporated into the equivalent circuit [15]. Fig. 6(A) illustrates the equivalent circuit model employed to simulate the resultant spectra of Pt and MWCNT CEs, and Fig. 6(B) illustrates the equivalent circuit models

Table 1
Best-fit values of R_S, W_{cat}, Y_{CPE}, R_{CT}, and W for the impedance spectra in Fig. 4, and the photovoltaic parameters of DSCs with different CEs.

	R_S (Ω cm^2)	W_{cat} (Ω cm^2)	Y_{CPE} (mF cm^{-2})	R_{CT} (Ω cm^2)	W (Ω cm^2)	E_{pp} (mV)	J_{SC} (mA cm^{-2})	V_{OC} (mV)	FF	η (%)
(a)	8.65		0.24	1.51	1.63	265	11.94	745	0.68	6.05
(b)	10.07		2.42	3.15	8.36		7.81	543	0.49	2.08
(c)	9.44	0.55	2.15	2.42	3.13	398	12.22	718	0.59	5.18
(d)	9.02	0.48	3.59	2.08	2.91	292	13.53	721	0.64	6.24

employed to simulate the resultant spectra of PANI and MWCNT/PANI CEs. These parameters were determined by fitting the impedance spectra using the Z-view software, and good agreement between the measured and the fitted data was achieved for all cases. The impedance parameters were listed in Table 1. Owing to the symmetric configuration of the dummy cell, the real R_{CT} value was calculated as half of the value obtained from the Z-view fitting. The R_{CT} increases in the order of Pt (1.51 Ω cm^2) < PANI/MWCNT (2.08 Ω cm^2) < PANI (2.42 Ω cm^2) < MWCNT (3.15 Ω cm^2), indicating an inverse order of electrocatalytic activity [33,34]. Additionally, the CPE magnitude (Y_{CPE}) increases in the order of Pt (0.24 mF cm^{-2}) < PANI (2.15 mF cm^{-2}) < MWCNT (2.42 mF cm^{-2}) < PANI/MWCNT (3.59 mF cm^{-2}). Basically, the larger Y_{CPE} value corresponds to larger active surface area, thus providing higher current response for the I_3^- reduction reaction and implying a higher electrocatalytic capability of this material. Nevertheless, there is an exceptional case for the MWCNT CE (discussed at the previous CV section). These findings are in accordance with the FE-SEM and CV results.

The Warburg impedance arises from limitations in the mass transportation of the electrolyte, especially when considering its transport in the PANI film, cannot be ignored. The term, W_{cat}, is not incorporated in the equivalent circuit for the Pt and MWCNT CEs. However, because of the increased film thickness for the PANI and PANI/MWCNT CEs, the diffusion length and resisting force for the I^- or I_3^- diffusing to or away from the PANI or PANI/MWCNT surface during the reaction are consequently increased. On the other hand, the porous structure of the PANI or PANI/MWCNT (as revealed by the FE-SEM image) effects on the reactant diffusion during the redox reaction. Therefore, the W_{cat} in the catalyst could not be ignored, and the Warburg impedance of the electrolyte increased. But even so, the PANI/MWCNT CE had relatively lower W_{cat} (0.48 Ω cm^2) and W (2.91 Ω cm^2) compared to the PANI CE.

Fig. 7 shows Tafel polarization curves to confirm the electrocatalytic activities of the Pt, MWCNT, PANI, and PANI/MWCNT CEs. Theoretically, the curve at the relatively low potential but higher than 0.10 V corresponds to the Tafel zone, where voltage (E), a linear function of the logarithm of the current density (lg J), is given by Eqn. (1), where R is the gas constant, T is the temperature, J^0 is the exchange current density, α is the distribution coefficient, F is Faraday's constant, and n is the number of electrons involved in the reaction at the electrode. The slopes for the anodic or cathodic branches are in the order of Pt > PANI/MWCNT > PANI > MWCNT. A steep slope of the Tafel zone indicates a large J^0, implying a relatively higher electrocatalytic activity [35]. J^0 can be also calculated by Eqn. (2), where R_{CT} is the charge-transfer resistance obtained from EIS spectra (Fig. 5). Apparently, the calculated J^0 also follows the order of Pt > PANI/MWCNT > PANI > MWCNT. As a result, the investigation for the electrocatalytic activity derived from the Tafel polarization and EIS data is well consistent.

$$E = \frac{2.3RT(\lg J - \lg J^0)}{\alpha nF} \quad (1)$$

$$R_{CT} = \frac{RT}{nFJ^0} \quad (2)$$

Fig. 8 compares the photovoltaic characteristics of DSCs based on various CEs under full sunlight illumination (100 mW cm^{-2}, AM1.5 G), and the resultant photovoltaic parameters are also summarized in Table 1. The J_{SC} value of the PANI/MWCNT CE was highest among all CEs, this might be owing to the highest cathodic current density, as indicated in the CV tests [36,37]. Generally, the V_{OC} value depends on the difference between the Fermi level of the electron in TiO_2 and the formal potential of the redox couples on the CE [1,2]. Because the TiO_2 photoanodes and the compositions of

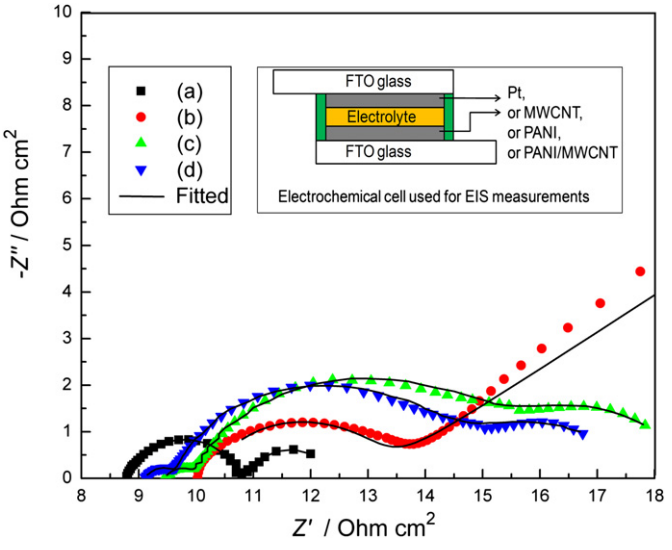

Fig. 5. Nyquist plots of the symmetrical (a) Pt, (b) MWCNT, (c) PANI, and (d) PANI/MWCNT CEs, respectively.

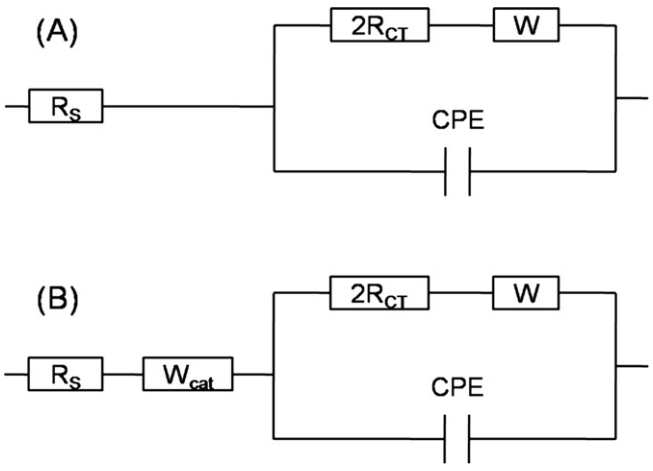

Fig. 6. Equivalent circuits used for simulating the obtained EIS results.

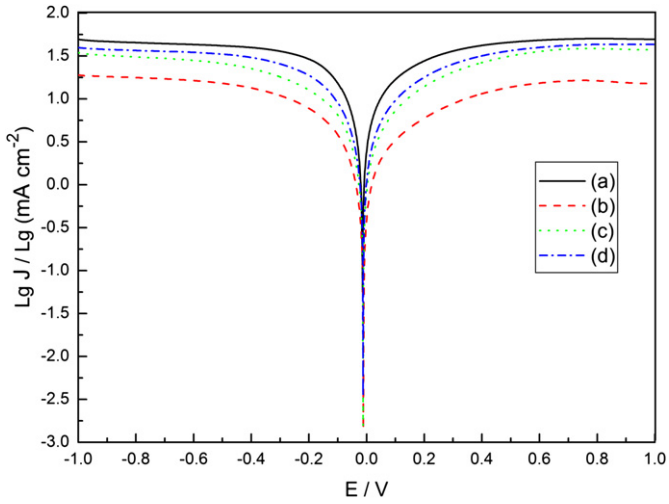

Fig. 7. Tafel curves of the symmetrical (a) Pt, (b) MWCNT, (c) PANI, and (d) PANI/MWCNT CEs, respectively.

the electrolytes for all of the DSCs are the same, the V_{OC} value of each DSC is mainly dependent on the electrochemical properties of the CE. It can be seen that the V_{OC} value of the DSC based on the Pt CE (745 mV) is the highest among all of DSCs in this study. This fact would be attributed to the cathodic peak potential of the reduction reaction on the Pt CE is the most positive among that all of the CEs (shown in Fig. 4), which resulting in a highest V_{OC} value [38]. However, because of the very high electrochemical activity, the PANI/MWCNT CE still possessed a relatively higher V_{OC} value (721 mV) than that of the PANI CE (718 mV). Moreover, the FF of the DSC assembled with the PANI/MWCNT CE (0.64) was higher than that of with the PANI CE (0.59), but lower than that of with the Pt CE (0.68). This can be attributed to its lower R_S and R_{CT} values (9.02 and 2.08 Ω cm^2, respectively) than those of the PANI CE (9.44 and 2.42 Ω cm^2, respectively), but higher than those of the Pt CE (8.65 and 1.51 Ω cm^2, respectively) [34,36,39]. Even so, the DSC with PANI/MWCNT CE exhibited a higher cell efficiency of 6.24% than that using Pt CE (6.05%) due to its enhanced J_{SC} value from the increased active surface area.

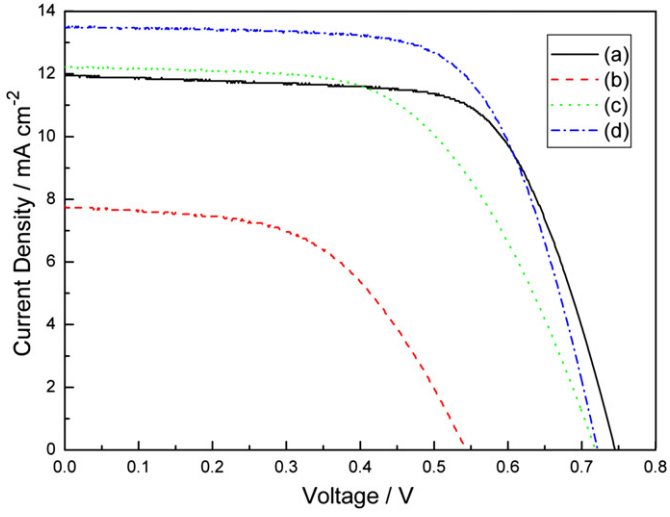

Fig. 8. Photocurrent density–voltage characteristics of the (a) Pt, (b) MWCNT, (c) PANI, and (d) PANI/MWCNT CEs, respectively.

4. Conclusions

In summary, high performance PANI/MWCNT was successfully deposited onto the MWCNT and FTO glass substrate through a pulse potentiostatic polymerization. 45 nm in thickness of PANI film can be obtained under 1.1 V pulse-on potential, 0 V pulse-reversal potential, 1 s pulse-on period, 0.5 s pulse-reversal period, and total 150 duration time. The PANI/MWCNT CE exhibited amazing electrocatalytic activity for the reduction of I_3^- due to its high cathodic current density in the CV test and the low R_{CT} of 2.08 Ω cm^2, and the DSC with it produced a higher J_{SC} value than that using the Pt CE. Therefore, the DSC assembled with the PANI/MWCNT CE exhibited superior power conversion efficiency to that with the Pt CE. In view of this facile approach, low-cost, and highly electrochemical catalysts, the PANI/MWCNT CE demonstrates a promising potential in production of large-scale DSCs.

Acknowledgment

The authors are very grateful to the National Science Council in Taiwan for its financial supports under contract no. NSC-101-2221-E-036-035.

References

[1] B. O'Regan, M. Grätzel, Nature 353 (1991) 737.
[2] M. Grätzel, Inorg. Chem. 44 (2005) 6841.
[3] M. Grätzel, Acc. Chem. Res. 42 (2009) 1788.
[4] M. Grätzel, Nature 414 (2001) 338.
[5] A. Hagfeldt, G. Boschloo, L. Sun, L. Kloo, H. Pettersson, Chem. Rev. 110 (2010) 6595.
[6] G. Smestad, C. Bignozzi, R. Argazzi, Sol. Energy Mater. Sol. Cells 32 (1994) 259.
[7] A. Kay, M. Grätzel, Sol. Energy Mater. Sol. Cells 44 (1996) 99.
[8] E. Ramasamy, W.J. Lee, D.Y. Lee, J.S. Song, Electrochem. Commun. 10 (2008) 1087.
[9] J.M. Pringle, V. Armel, D.R. MacFarlane, Chem. Commun. 46 (2010) 5367.
[10] K.S. Lee, H.K. Lee, D.H. Wang, N.G. Park, J.Y. Lee, O.O. Park, J.H. Park, Chem. Commun. 46 (2010) 4505.
[11] J.H. Wu, Q.H. Li, Z. Lan, P.J. Li, J.M. Lin, S.C. Hao, J. Power Sources 181 (2008) 172.
[12] S.S. Jeon, C. Kim, J. Ko, S.S. Im, J. Mater. Chem. 21 (2011) 8146.
[13] N. Ikeda, T. Miyasaka, Chem. Commun. 16 (2006) 1733.
[14] K.C. Huang, J.H. Huang, C.H. Wu, C.Y. Liu, H.W. Chen, C.W. Chu, J.T. Lin, C.L. Lin, K.C. Ho, J. Mater. Chem. 21 (2011) 10384.
[15] J. Chen, B. Li, J. Zheng, J. Zhao, H. Jing, Z. Zhu, Electrochim. Acta 56 (2011) 4624.
[16] Y. Xiao, J.Y. Lin, S.Y. Tai, S.W. Chou, G. Yue, J. Wu, J. Mater. Chem. 22 (2012) 19919.
[17] C.E. Banks, R.G. Compton, Analyst 131 (2006) 15.
[18] J.Y. Lin, J.H. Liao, T.Y. Hung, Electrochem. Commun. 13 (2011) 977.
[19] G.R. Li, Q.W. Jiang, X.P. Gao, P.W. Shen, Angew. Chem. Int. Ed. 49 (2010) 3653.
[20] S.S. Kim, Y.C. Nah, Y.Y. Noh, J. Jo, D.Y. Kim, Electrochim. Acta 51 (2006) 3814.
[21] M.C. Tsai, T.K. Yeh, C.H. Tsai, Electrochem. Commun. 56 (2011) 8545.
[22] Y.M. Xiao, J.H. Wu, G.T. Yue, J.M. Lin, M.L. Huang, Z. Lan, Electrochim. Acta 56 (2011) 8545.
[23] J.Y. Lin, J.H. Liao, S.W. Chou, Electrochim. Acta 56 (2011) 8818.
[24] J.H. Wu, Z. Lan, J.M. Lin, M.L. Huang, S.C. Hao, T. Sato, S. Yin, Adv. Mater. 19 (2007) 4006.
[25] J.H. Wu, Y.M. Xiao, G.T. Yue, Q.W. Tang, J.M. Lin, M.L. Huang, Y.F. Huang, L.Q. Fan, Z. Lan, S. Yin, T. Sato, Adv. Mater. 24 (2012) 1884.
[26] T. Saleh, S. Agarwal, V. Gupta, Appl. Catal. B Environ. 106 (2011) 45.
[27] J. Kathi, K.Y. Rhee, J. Mater. Sci. 43 (2008) 33.
[28] G. Wang, W. Xing, S. Zhuo, Electrochim. Acta 66 (2011) 151.
[29] Z. Huang, X.Z. Liu, K.X. Li, D.M. Li, Y.H. Luo, H. Li, W.B. Song, L.Q. Chen, Q.B. Meng, Electrochem. Commun. 9 (2007) 596.
[30] J. Roy-Mayhew, D. Bozym, C. Punckt, I. Aksay, ACS Nano. 4 (2010) 6203.
[31] T.N. Murakami, S. Ito, Q. Wang, M.K. Nazzeruddin, T. Bessho, I. Caser, P. Liska, R. Humphry Baker, P. Comte, P. Péchy, M. Grätzel, J. Electrochem. Soc. 153 (2006) A2255.
[32] X. Wu, H. Ma, S. Chen, Z. Xu, A. Sui, J. Electrochem. Soc. 146 (1999) 1847.
[33] A. Fujiwara, Y. Matsuoka, Y. Matsuoka, H. Suematsu, N. Ogawa, K. Miyano, H. Kataura, Y. Maniwa, S. Suzuki, Y. Achiba, Carbon 42 (2004) 919.
[34] G. Mor, K. Shankar, M. Paulose, O. Varghese, C. Grimes, Nano Lett. 6 (2006) 215.
[35] M. Wang, A.M. Anghel, B. Marsan, N.-L. Cever Ha, N. Pootrakulchote, S.M. Zakeeruddin, M. Grätzel, J. Am. Chem. Soc. 131 (2009) 15976.
[36] Y. Saito, W. Kubo, T. Kitamura, Y. Wada, S. Yanagida, J. Photochem. Photobiol. A 164 (2004) 153.
[37] J. Lin, J. Liao, J. Electrochem. Soc. 159 (2012) D65.
[38] K. Imoto, K. Takahashi, T. Yamaguchi, T. Komura, J. Nakamura, K. Murata, Sol. Energy Mater. Sol. Cells 79 (2003) 459.
[39] E. Ramasamy, W.J. Lee, D.Y. Lee, J.S. Song, J. Power Sources 165 (2007) 446.